Apolar and polar transitions drive the conversion between amoeboid and mesenchymal shapes in melanoma cells

Sam Cooper[a,b], Amine Sadok[a], Vicky Bousgouni[a], and Chris Bakal[a]
[a]Division of Cancer Cell Biology, Institute of Cancer Research, Chester Beatty Laboratories, London SW3 6JB, United Kingdom; [b]Department of Computational Systems Medicine, Imperial College, London, South Kensington Campus, London SW7, United Kingdom

ABSTRACT **Melanoma cells can adopt two functionally distinct forms, amoeboid and mesenchymal, which facilitates their ability to invade and colonize diverse environments during the metastatic process. Using quantitative imaging of single living tumor cells invading three-dimensional collagen matrices, in tandem with unsupervised computational analysis, we found that melanoma cells can switch between amoeboid and mesenchymal forms via two different routes in shape space—an apolar and polar route. We show that whereas particular Rho-family GTPases are required for the morphogenesis of amoeboid and mesenchymal forms, others are required for transitions via the apolar or polar route and not amoeboid or mesenchymal morphogenesis per se. Altering the transition rates between particular routes by depleting Rho-family GTPases can change the morphological heterogeneity of cell populations. The apolar and polar routes may have evolved in order to facilitate conversion between amoeboid and mesenchymal forms, as cells are either searching for, or attracted to, particular migratory cues, respectively.**

Monitoring Editor
Leah Edelstein-Keshet
University of British Columbia

Received: Jun 15, 2015
Revised: Aug 10, 2015
Accepted: Aug 12, 2015

INTRODUCTION

Melanoma metastasis is driven by changes in tumor cell shape that allow cells to invade adjacent tissues, disseminate through the circulatory system, and colonize distant organs (Friedl and Alexander, 2011). Although the acquisition of a metastatic phenotype had long been considered to involve a single-phase transition from a nonmigratory to a migratory shape, such as epithelial to mesenchymal (Nieto, 2013), it is now clear that migratory modes are highly diverse in nature. For example, in three-dimensional (3D) environments, individual metastatic melanoma cells appear to adopt a "mesenchymal" or "amoeboid" shape, depending on cell-extrinsic (e.g., elasticity of the extracellular environment) and cell-intrinsic (e.g., gene expression) factors (Friedl and Wolf, 2003; Sahai and Marshall, 2003; Sanz-Moreno *et al.*, 2008, 2011). In contrast, melanoma cells cultured on two-dimensional (2D) plastic surfaces typically adopt a spread/flattened shape that bears little resemblance to the forms adopted in vivo (Yin *et al.*, 2013). Amoeboid and mesenchymal forms migrate in 3D environments using distinct mechanisms. In general, mesenchymal forms migrate through cycles of protrusion, adhesion, and retraction (Parsons *et al.*, 2010). In contrast, amoeboid forms migrate in three dimensions by squeezing through gaps in the extracellular matrix (ECM), using different forms of membrane blebbing, in an adhesion-independent manner (Friedl and Wolf, 2003; Sahai and Marshall, 2003; Tozluoglu *et al.*, 2013; Liu *et al.*, 2015). Signaling pathways promoting amoeboid or mesenchymal shapes have been elucidated in melanoma cells. The GTPase Rac1, activated by a NEDD9-DOCK3 complex, promotes mesenchymal morphogenesis via WAVE2-mediated actin polymerization. In contrast, Rho-associated protein kinases 1 and 2 (ROCK1 and ROCK2), which likely act downstream of RhoA and/or RhoC (Sanz-Moreno *et al.*, 2008; Acton *et al.*, 2014), up-regulate actomyosin contractility and promote amoeboid morphogenesis. ROCK signaling can antagonize Rac1 activity via ARHGAP22, a

This article was published online ahead of print in MBoC in Press (http://www.molbiolcell.org/cgi/doi/10.1091/mbc.E15-06-0382) on August 26, 2015.

Address correspondence to: Sam Cooper (sc2011@ic.ac.uk), Chris Bakal (chris.bakal@icr.ac.uk).

Abbreviations used: DBI, Davies–Bouldin index; ECM, extracellular matrix; GMM, Gaussian mixture model; PCA, principal component analysis; SC, shape cluster; SCP, shape cluster profile.

Rac1 inhibitor, and Rac1-WAVE can antagonize ROCK signaling (Sanz-Moreno *et al.*, 2008). Identification of the amoeboid and mesenchymal shapes and signaling pathways that promote these shapes has led to the attractive notion that suppression of these pathways may inhibit metastasis.

The amoeboid–mesenchymal model of morphogenesis provides an important starting point for gaining insights into melanoma metastasis, but the question of whether melanoma cells have only two forms in 3D matrices remains open. Moreover, although there have been recent advances in describing how changes in environmental conditions, or cell-extrinsic factors, cause amoeboid and mesenchymal transitions (Tozluoglu *et al.*, 2013; Liu *et al.*, 2015), much remains to be understood regarding transitions between amoeboid and mesenchymal forms in relatively constant environments and how cell-intrinsic factors drive transitions. For example, we showed that, when cultured in 3D environments, in the absence of stimulation, melanoma cells reversibly switch between amoeboid and mesenchymal forms. Our work implicated PTEN as a regulator of the transition rates between mesenchymal and amoeboid forms, but how signal transduction regulates transition dynamics and not amoeboid or mesenchymal morphogenesis per se is not clear (Yin *et al.*, 2013). Moreover, because previous studies mainly performed imaging of fixed cells in three dimensions using qualitative assignment of shape, melanoma shape space has not been quantitatively described, let alone how this space is explored over time. Because the ability of melanoma cells to transition between forms underpins the morphological heterogeneity of populations, which can itself be a driver of disease (Almendro *et al.*, 2013), gaining insight into transition dynamics may be clinically relevant.

To quantify systematically the shape space of melanoma cells and characterize the regulation of their morphogenesis, we analyzed single-cell shape dynamics of live cells cultured in 3D collagen matrices using an unsupervised approach. Unsupervised methods free the analysis of any prior bias regarding the number of morphologies that may be present in any population. That is, we did not wish to presume the existence of even well-characterized amoeboid and mesenchymal shapes before we began this analysis. Using unsupervised methods, we show that melanoma cells in three dimensions do exist primarily in amoeboid or mesenchymal shapes as suggested by qualitative studies, but we also observe additional shapes that are adopted as cells transition between mesenchymal and amoeboid forms using two distinct routes. We term these the apolar and polar routes. Melanoma cells transition between amoeboid and mesenchymal shapes and vice versa using both routes. We propose that the routes evolved to ensure that transitions between phenotypically distinct states are robust to environmental and genetic flux, especially changes in ECM stiffness and geometry. After gene depletion of Rho-family GTPases, cells can be biased to transition via one route versus another. Critically, in these studies, we did not seek to provide specific mechanistic insights into how different GTPases regulate specific morphologies, but instead aimed at determining previously undefined constraints that have to be satisfied in functional studies regarding the role of individual Rho-family members.

RESULTS

To describe the shape space explored by melanoma cells, we cultured WM266.4 melanoma cells on top of thick 3D fibrillar bovine collagen I matrices that mimic the elasticity and geometry of soft tissues in vivo (Sanz-Moreno *et al.*, 2008). We chose WM266.4 cells because on soft matrices these cells exist in ~50:50 mixtures of amoeboid and mesenchymal forms (Sahai and Marshall, 2003; Yin *et al.*, 2013) and exhibit frequent transitions that occur on minute time scales between amoeboid and mesenchymal shapes (Yin *et al.*, 2013). Thus WM266.4 cells are an excellent cell type with which to study the morphological heterogeneity and interconversion between shapes in three dimensions. In contrast, other melanoma lines, such as A375m2, appear to switch between rounded and mesenchymal forms at much slower (hours) frequency (Sanz-Moreno *et al.*, 2008) and are often mostly amoeboid in soft collagen (Sahai and Marshall, 2003).

Cells were plated on top of 300–700 μM matrices of 1.7 mg/ml collagen I. We estimated the elastic modulus of the matrix on the top of the gel to be ~200 Pa (Paszek *et al.*, 2005); this is considered a "soft" matrix, with stiffness similar to lung tissue (Butcher *et al.*, 2009). To quantify the largest possible morphological space explored by melanoma cells in three dimensions in the minimal number of experiments, we generated a data set in which we depleted Rho-family GTPases using RNA interference (RNAi). Our previous work demonstrated that gene depletion rarely results in new shapes but instead enriches for shapes that are present in small numbers in wild-type cells; thus we reasoned that the shape space wild-type melanoma cells explore in three dimensions can be defined by leveraging this enrichment (Yin *et al.*, 2013; Sailem *et al.*, 2014). Because Rho-family GTPases are well-known cell shape regulators (Jaffe and Hall, 2005), we predicted that their depletion would result in us observing the majority of shapes that a melanoma cell might assume. We emphasize that systematic RNAi depletion is used primarily to generate morphological diversity rather than as a means by which to identify "hits," as in classical genetic screens. After live high-throughput 2D confocal imaging (Supplemental Movie S1), automated cell segmentation and filtering was performed (see *Materials and Methods*), and 15 features describing cell shape were recorded, forming the data set used for analysis. Cells were imaged soon (8–20 h) after being cultured on top of the matrix. There is no chemoattractant to promote invasion "downward" along the *z*-axis into the matrix, and thus most cells explore shape space primarily along the *x*-and *y*-axes, and we believe that the 3D morphology of cells is well approximated by 2D confocal imaging. Across all time points, 62,000 cell segments were recorded, with 423 being the minimum number recorded for a well. Static analysis was also performed on random samples of 400 cells/well taken from live-cell imaging.

Characterizing melanoma shape space

Supervised methods have proven useful to identify distinct cell morphologies (Boland and Murphy, 2001; Bakal *et al.*, 2007; Jones *et al.*, 2009; Ramo *et al.*, 2009). However, such methods require human intervention and thus are prone to bias. Recently we developed an unsupervised method (Sailem *et al.*, 2014) to characterize shape space based on the mean silhouette statistic (Rousseeuw, 1987). In this previous study, we initially performed principal component analysis (PCA). After performance of clustering of the first three principal components using Gaussian mixture models (GMMs), calculation of the maximum silhouette score defined the number of shapes adopted by *Drosophila* BG-2 cells (Sailem *et al.*, 2014).

Here we sought to describe the shape space explored by melanoma cells by identifying clusters of similarly shaped cells, termed "shape clusters" (SCs). We first attempted to use PCA followed by GMM clustering, as we did previously (Sailem *et al.*, 2014). However, PCA followed by GMM resulted in no clear maximum silhouette value, and we could not unambiguously identify the number of shapes in the data set. This could be a result of the transformation (PCA) and clustering (GMM) method or the cells themselves (i.e., the cells might not assume quantitatively different shapes). To explore

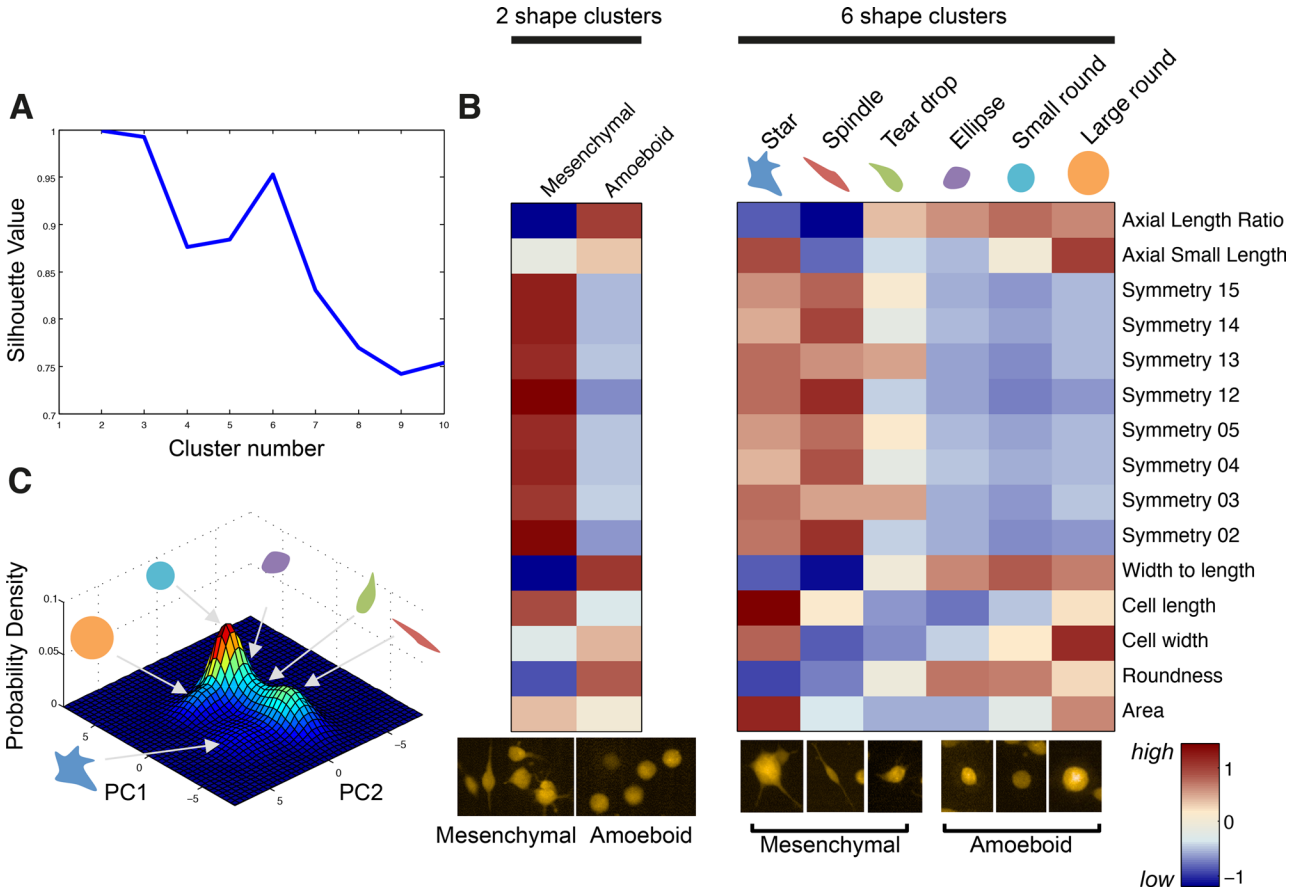

FIGURE 1: Melanoma cells adopt six shapes in 3D soft collagen matrices. (A) The stability score over cluster numbers 2–10, calculated as the silhouette value applied to *k*-means clustering of centroids. Centroids are from 100 resamples of initial *k*-means clustering to identify shape clusters (SCs) from a sample of 2000 cells. This measure is designed to identify a cluster number that gives reproducible clustering of the data set. (B) Heat maps of normalized feature values were averaged for each SC. Below the heat maps are images of cells summarizing each cluster. Round shapes correspond to low symmetry and high roundness/width:length scores. The teardrop shape scores stronger for odd symmetry measures, whereas the spindle/mesenchymal shape is stronger for even symmetry measures and the large star shape scores high for all measures, except roundness/width:length. (C) PCA was applied to a pooled sample of 2000 cells; the mean and SD for the first two PCs (77% of variance) are then plotted as a normal distribution scaled to cluster membership for wild-type cells.

the former possibility, we sought to develop an alternate unsupervised method based on cluster stability (Shamir and Tishby, 2008; von Luxburg, 2010; Bubeck *et al.*, 2012).

We first sought to identify the best method to transform and cluster our data that did not involve any assumptions regarding the result, that is, assuming that there are a limited number of distinct shapes present in the population. To measure how well an unsupervised method is performing, we use the Davies–Bouldin index (DBI; Davies and Bouldin, 1979) to quantify how similar shape distributions are between experimental repeats (where the same small interfering RNA [siRNA] is used to target the same gene in different transfections) and how different they are between knockdowns. Methods with a low DBI value identify shapes that maximize the differences in cell shape distribution across gene knockdowns and minimize differences within experimental repeats of a knockdown. This use of the DBI is similar to a separation statistic used to determine how effectively methods identified shapes in *Caulobacter*, Madin–Darby canine kidney cells, and keratocytes (Pincus and Theriot, 2007).

The data transformation that results in the lowest DBI (see *Materials and Methods* and Supplemental Information) bins feature values into binary values based on the mean feature value (1 for above and 0 for below) of a 2000-cell sample stratified across all wells. After this transformation, *k*-means, fuzzy *C*-means, and hierarchical clustering all perform equally well at identifying distinct shapes, or clusters, within the population (Supplemental Figure S2). We found that *k*-means was the fastest computationally, and therefore we subsequently used this procedure. To determine the number of shapes/clusters that best describes the data set as a whole in an unsupervised manner, we again calculated the silhouette value across a range of cluster numbers on the transformed data, but still no maximum silhouette score emerged (Supplemental Figure S3A). However, by using the silhouette index to measure how stable clustering is over resampling (Shamir and Tishby, 2008; von Luxburg, 2010), calculating what we term here the "stability score," we found clear maxima at two or six shapes (Figure 1A and Supplemental Information), corresponding to stable cluster centroids (Figure 1B). By looking at the feature values of each SC's centroid (Figure 1C) and images enriched for an SC, an understanding of the shapes present in that SC emerges. When clustered as two shapes, SC_1 is comprised of mesenchymal shapes defined by "high-symmetry" and "low-length-to-width" features. SC_1 is typified by protrusive bipolar

cells with long protrusions that are symmetrical about all axes. SC_2 comprises cells with amoeboid shapes and is identified by "high-roundness" and "low-symmetry" features (Figure 1C). The low symmetry of these cells is due to the fact that most cells in this category, although rounded, are not perfectly round, likely due to the presence of small protrusions and blebs. These two SCs support the well-established idea that melanoma cells in three dimensions exist in amoeboid and mesenchymal shapes (Sahai and Marshall, 2003; Sanz-Moreno *et al.*, 2008; Friedl and Wolf, 2009; Yin *et al.*, 2013).

Considering six shapes, we see three forms that, although quantitatively distinct, would normally be qualitatively classed as amoeboid ("large round," "small round," and "ellipse" shapes) and another three that would be considered mesenchymal ("teardrop," "spindle," and "star" shapes; Figure 1B). By plotting the frequency distributions of the six shapes in wild-type populations in 2D PC space, we observe that the small round and ellipse shapes are closely related and together represent the predominant shapes adopted in three dimensions by wild-type melanoma cells (Figure 1C). Together, we consider the small round and ellipse shapes to be the classically defined amoeboid form (Sahai and Marshall, 2003). Although qualitatively similar to amoeboid shapes, large round cells are quantitatively distinct, and it is likely that these cells have been misclassified in previous studies in which shape classification was performed by human observers. Of note, these cells do not appear to forms blebs, suggesting that they are round but not contractile. The second-most-predominant shape is the spindle shape, which would classically be defined as mesenchymal (Figure 1C). The star-shaped and teardrop-shaped cells appear to be rare forms that exist between amoeboid and mesenchymal in shape space. Previous studies classified multiprotrusive, star-like shapes as mesenchymal (Sanz-Moreno *et al.*, 2008). Thus our unsupervised analysis characterized the shape space explored by melanoma cells in 3D soft collagen. In agreement with previous qualitative studies, rounded and spindle shapes are the dominant shapes in populations, but we see that additional shapes are indeed present in both wild-type cells and are enriched in populations in which Rho-family GTPases have been systematically depleted.

Effects of gene depletion on the exploration of shape space

By analyzing how gene depletion alters the distribution of single-cell shapes, we assign gene depletions a "shape cluster profile" (SCP; a generalization of the Treatment Condition Heterogeneity Profile in Sailem *et al.* [2014])—specifically, a unit vector with elements (one for each SC) giving the fraction of cells classified into an SC. An SCP describes the morphological heterogeneity present in a population.

Hierarchical clustering of SCPs results in four groups with different shapes at the population level (Figure 2A). Images of representative knockdowns for these groups are shown in Figure 2B. In all cases, depletion results in heterogeneous populations, although populations and clusters are often enriched for one or two shapes. The largest group of SCPs, which we term "transitional," is enriched

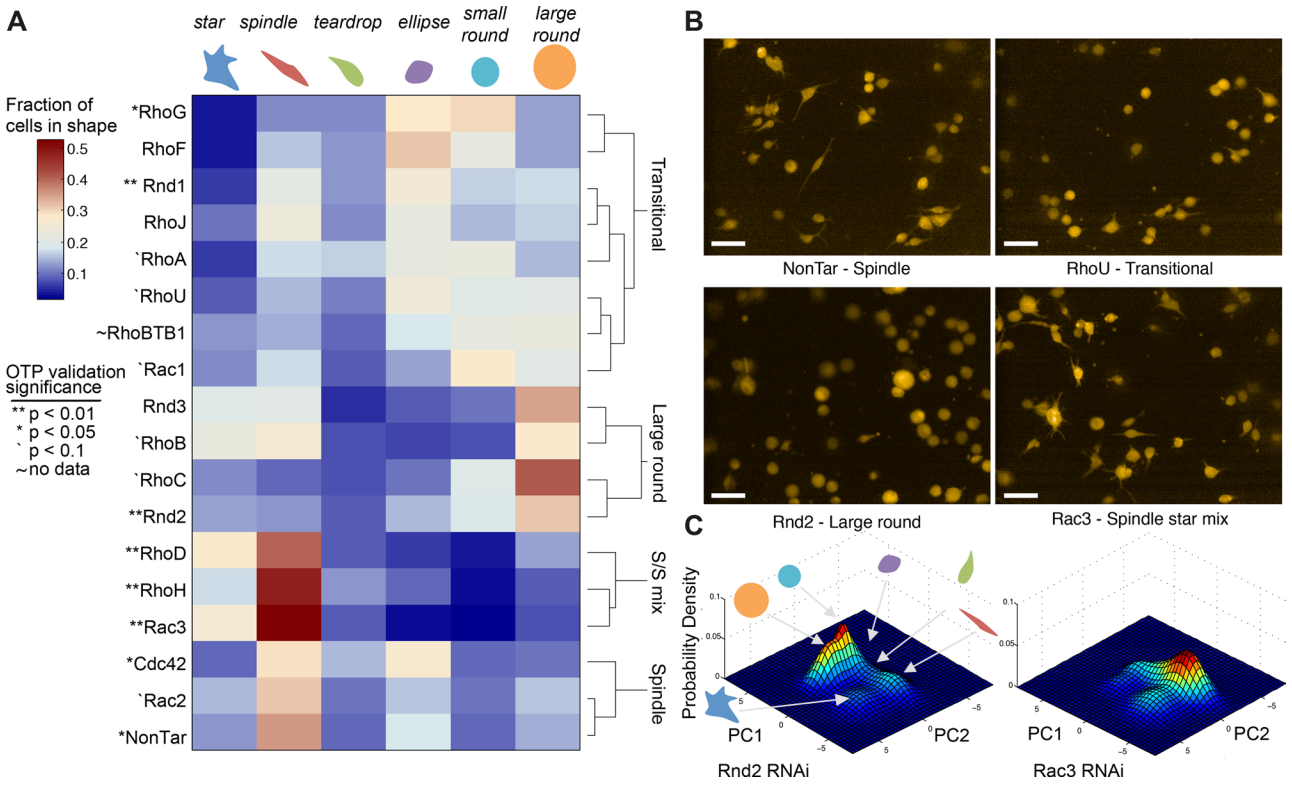

FIGURE 2: Rho-family GTPases regulate the exploration of shape space in 3D matrices. (A) Hierarchical clustering of genes based on shape cluster profiles (SCPs), which define the fraction of cells in a shape cluster (SC) averaged over repeats. Wards linkage was used for clustering, with a cut-off value of 0.3 (maximum distance 1). Validations with individual OTP siRNAs was performed and *p* values for the best validating siRNA against a null distribution are displayed. (B) Images of representative knockdowns for the four groups. Scale bars, 50 μm. (C) Frequency distribution of Rnd1-depleted cells (left) and Rac3-depleted cells (right). Rnd1-depleted cells are enriched in large round cells, and Rac3 is enriched in spindle-shaped cells. The distribution of wild-type cells is shown in Figure 1B.

for ellipse and teardrop shapes while having very few star shapes. Rac1 or RhoG depletion results in a transitional phenotype consistent with previous studies showing that Rac1 is required for protrusion and inhibition induces rounding in HT1080 cells in a 3D collagen matrix (Sanz-Moreno *et al.*, 2008; Yamazaki *et al.*, 2009) and that RhoG can promote Rac1 activity and polarized protrusions (Damoulakis *et al.*, 2014). Like Rac1 depletion, RhoA depletion also results in a transitional phenotype, but RhoA is part of a subcluster that is phenotypically distinct from the Rac1- or RhoG-depleted cells. RhoA depletion results in a weakly penetrant phenotype in which there is a small increase in spindle, teardrop, and ellipse shapes compared with wild-type cells (Figure 2A).

The second group has increased numbers of large round cells. Of note, Rnd2 (Figure 2C), Rnd3, and RhoB fall into this group, agreeing with evidence that Rnd2 and Rnd3 activate RhoB in endothelial cells (Gottesbuhren *et al.*, 2013). Because the Rnd2/3–RhoB axis promotes contractility (Gottesbuhren *et al.*, 2013), this supports the idea that loss of contractility may lead to the large round shape and an inability to generate blebs similar to highly contractile small round cells. This is in contrast to small round and ellipse-shaped cells, in which contractility is high. The third group is enriched for star and spindle shapes. Rac3, RhoH, and RhoD depletions are in this group, suggesting a role for these GTPases in suppressing protrusions and/or adhesion, thereby promoting amoeboid morphogenesis. In fact Rac3 promotes rounding, weakens adhesions, and blocks neurite outgrowth in neuronal cells (Hajdo-Milasinovic *et al.*, 2007, 2009). The final group is enriched in spindle shapes, but no shape is notably reduced. The wild-type cell population features in this group; this agrees with our findings that wild-type populations generally contain the full range of shapes that cells adopt, although often at low levels.

Of note, our analysis reveals that depletion of RhoA, RhoB, or RhoC leads to distinct single-cell and population-level phenotypes. Thus, although RhoA, RhoB, and RhoC are structurally very similar and share activators and effectors, they are not functionally redundant regarding their regulation of cell shape. Our findings are in line with several studies showing diverse roles for these proteins (Ridley, 2013). Similarly, Rac1, Rac2, and Rac3 have very diverse functions based on our analysis, despite their similarity and shared activators/effectors, consistent with the idea they have unique functions (Gu *et al.*, 2003; Wheeler *et al.*, 2006).

To validate the siGENOME RNAi pool data set, we depleted all Rho GTPases using four individual OnTargetPlus (OTP) siRNAs (full results in the Supplemental Information). All six shapes present in the siGENOME data set were also in the OTP data set, supporting that we have well characterized the shape space explored by melanoma cells. We saw significant reproducibility in the phenotypes resulting from siGENOME and OTP siRNAs (Figure 2A and Supplemental Figure S4D).

Quantifying shape dynamically

To understand how melanoma cells explore shape space over time, we recorded the number of transitions cells make from one shape (as defined by membership in an SC) to another between 5-min time points in a matrix of all possible transitions, including shapes staying the same (transition to self). We divided the matrix of all transitions by the total number of transitions made for a gene knockdown; each matrix element is therefore the percentage of all transitions being made between two shapes defined by the row and column. We are likely not missing forms that would be seen by imaging at shorter time points, since after averaging over all transition matrices, we observe that transitions are much more frequently made between closely versus distantly related shapes (Figure 3A).

This analysis reveals the existence of two different routes between the amoeboid (here the small round and elliptical forms) and mesenchymal (spindle) forms. In one route, transitions between amoeboid and mesenchymal forms occur by polarized ellipse and teardrop intermediates—here termed the "polar" route. In contrast, cells also transition via the large round and star-shaped intermediates, which we term the "apolar" route. Although other transitions occur, these happen at a much lower frequency (Figure 3B). Of note, we see no directionality to shape transitions; the matrices are largely symmetrical about the diagonal, meaning that transitions between shapes are highly reversible (Figure 3A). Quantitatively, the sum of upper triangular elements divided by the sum of lower triangular elements (excluding diagonal) averaged over all gene depletions gives a ratio of 1.0028, with SD of 0.0098.

We find that gene depletion has specific effects on shape dynamics, as shown in the array of transition matrices (Figure 3D). To emphasize the effect of depletion on transitions, we calculate a "dynamic score" describing the number of transitions between shapes compared with shapes staying the same (Figure 3E). This is calculated as the sum of off-diagonal elements divided by the sum of diagonal elements; higher values mean that a population is more dynamic. The average value of this score is 0.5, that is, a single shape transition occurs in three frames (15 min). By hierarchical clustering of the transition matrices, gene depletions can be grouped into five major groups: 1) cells in which the polar route is enriched and mesenchymal morphogenesis is weakly compromised (Rnd1 RNAi); 2) cells in which mesenchymal morphogenesis is compromised (Rnd2 RNAi); 3) cells in which the apolar route is enriched and amoeboid morphogenesis is weakly compromised (RhoD RNAi); 4) cells with transition dynamics that are similar to wild type; and 5) cells in which amoeboid morphogenesis is compromised and the dynamic score is notably lower (Rac 3 RNAi). In cases in which gene depletion results in an enrichment of either polar or apolar transitions, we do not see a block in transitions via the other route, and the overall dynamic score is therefore higher (groups 1 and 3 generally have a higher dynamic score than groups 2, 4, and 5). A parsimonious explanation of how gene depletion can alter transition dynamics without greatly affecting amoeboid or mesenchymal morphogenesis is that these genes regulate the dynamics of cycling/oscillatory processes required for conversion between forms, such as adhesion turnover, microtubule dynamics, and actin flow, but are not essential for any particular process. Taken together, these data show that the depletion of Rho-family GTPases can either prevent mesenchymal or amoeboid morphogenesis (groups 3 and 5) or alter transition rates through the apolar or polar routes with less effect on the adoption of the mesenchymal or amoeboid morphogenesis per se (groups 1 and 3).

DISCUSSION

Describing the shape space explored by any cell type in a given environment is both a biological and data analysis challenge, but this is particularly so when describing the space explored in 3D environments, where the potential shape space that cells can explore expands and in which cells are difficult to image. However, because historically most studies have been done using cells cultured on 2D plastic tissue culture dishes, it is important to find means to understand cell morphogenesis in 3D systems that more closely resemble the environment that cells would encounter in vivo.

With regard to the analytical challenge of describing shape space, we find that binning continuous features into binary values

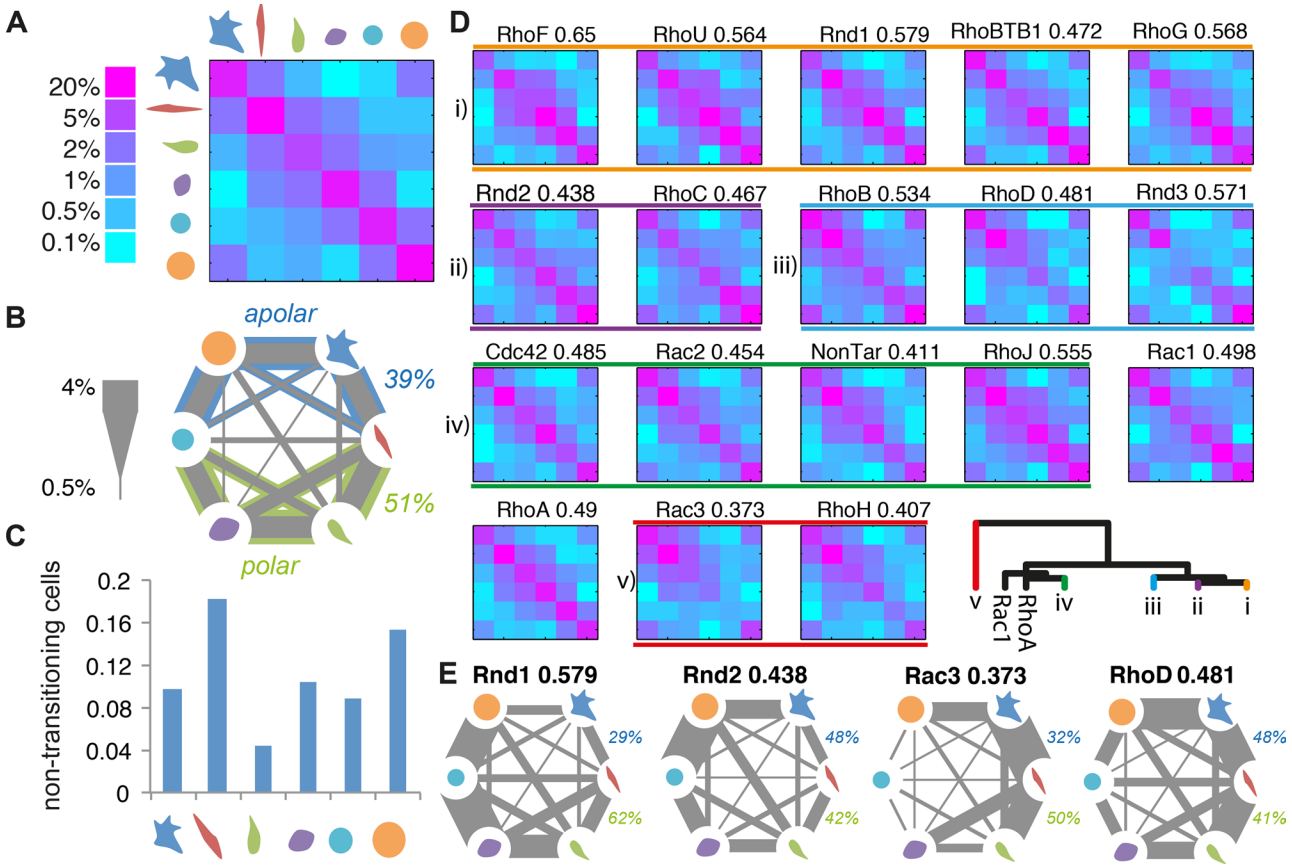

FIGURE 3: Melanoma cells transition between amoeboid and mesenchymal shapes using two distinct routes. (A) Heat map showing the percentage of transitions between shapes including to self (diagonal) averaged across all gene knockdowns; log-scale coloring. (B) Alternative visualization of the matrix shown in A. Weighted edges show the mean percentage of transitions made between shapes; the majority of transitions are made between "neighboring" shapes. The total joint probability (shown as percentage) of a cell going from small round to spindle via either route is given for a sense of the overall flux along each route; this is calculated as the sum of joint probabilities for the three possible ways of transitioning along either the polar or apolar route (see Supplemental Table S5 for individual joint probabilities). (C) Percentage of cells in a given shape staying in that shape. (D) Effect of depletion on the number of transitions being made; color as in A. In addition, off-diagonal values divided by diagonal values are given beside the gene name as a statistic of how dynamic a knockdown is, termed the "dynamic score." (E) Weighted graphs of four representative gene depletions, which emphasize how gene depletion affects dynamics. The dynamic score and route percentages based on joint probability are also shown for the example depletions.

beneficially transforms the data before identification of SCs; this is independent of SC number. By using measures of cluster stability to determine the number of SCs present in the data set in an unsupervised manner, we then minimize the bias in our quantification of the shape space explored by melanoma cells. This method is generalizable to quantification of cell shape in other studies, and we believe that it is also particularly amenable to noisy data sets, where clear clusters do not emerge. Here we find that melanoma cells exist as six different shapes. Of note, we cannot consider all these shapes as discrete forms, since no clear maximum emerged from measuring cluster membership.

We envision melanoma shape space as an energetic landscape where amoeboid and mesenchymal shapes exist as stable minima separated by barriers of potential. When cells overcome this barrier, this results in a switch-like transition between amoeboid and mesenchymal cells. There are two different routes by which this barrier can be overcome (Figure 4A). The first route is defined by "polar intermediates" and is used when polarity is maintained during transitions, for example, as cells are migrating toward chemoattractants and/or during "one-dimensional" migration, such as when migrating along collagen fibers (Doyle *et al.*, 2009). We propose that "group 1" genes such as Rnd1 promote switch-like transitions between the amoeboid and mesenchymal forms by acting as parts of signaling networks whose emergent behavior leads to the adoption of a single or multiple (e.g., bistable) shapes in the presence of polarizing cues. Thus loss of Rnd1 alters signaling network activity, leading to both increased transitions between amoeboid and mesenchymal shapes and the accumulation of intermediate polar forms as the transitions become less switch-like (Figure 4B). Of note, Rnd1 is a negative regulator of ERK signaling (Okada *et al.*, 2015), and we have demonstrated that ERK promotes rounding (Yin *et al.*, 2013). Increased ERK signaling in Rnd1-depleted cells could destabilize protrusions and/or lead to rapid interconversion between amoeboid and mesenchymal shapes, resulting in the accumulation of polar shapes. Of interest, Rnd1 depletion accelerates disease in mouse models of breast cancer (Okada *et al.*, 2015). Although the role of Rnd1 as a tumor suppressor has largely been attributed to increases in ERK signaling, it is tempting to speculate that the increased

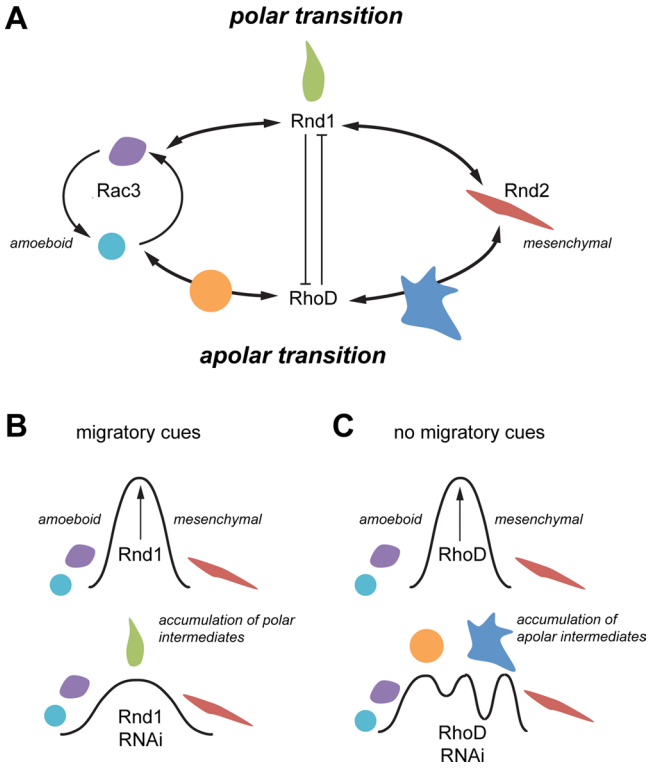

FIGURE 4: A model for shape transitions made by melanoma cells in 3D collagen matrix. (A) In this model, amoeboid (small round, ellipse) and mesenchymal shapes (spindle) can be considered regions of low potential in energetic space, whereas large round, star-shaped, and teardrop shapes are transitional/unstable forms. (B) To convert between amoeboid and mesenchymal shapes and maintain polarity, cells transition through a teardrop intermediate. Rnd1 activity promotes transitions through this route and thus is responsible for the height of the energetic barrier between amoeboid and mesenchymal shapes during the maintenance of polarity. Depletion of Rnd1 leads to the accumulation of teardrop intermediates and more frequent transitions because the energetic barrier is reduced. (C) In the apolar route, polarity is not maintained. RhoD is required to establish the height of the energetic barrier between amoeboid and mesenchymal shapes as cells transition along the routes. Depletion of RhoD leads to the accumulation of transitional forms and more frequent transitions. Rac3 is required for amoeboid morphogenesis. Rnd2 is required for mesenchymal morphogenesis. Rnd1 and RhoD may antagonize each other (Zanata *et al.*, 2002; Fansa *et al.*, 2013).

morphological heterogeneity resulting from the accumulation of polar intermediates could also drive disease.

In the apolar route, cells transition between a mesenchymal and large round form via the star shape, likely the result of cells with less polarity and contractility and increased adhesion (Figure 4C). We propose that cells transition between shapes using this route when polarity does not need to be maintained, such as in the absence of any chemoattractant. Based on the phenotypes of cells that accumulate in the apolar route ("group 3" genes), we propose that in three dimensions, a mesenchymal-to-amoeboid transition involves three processes: inhibition of protrusions, induction of contractility, and turnover of adhesions. In particular, RhoD depletion enriches for cells in this route as transitions become less switch-like. We postulate that this could be the result of reduced adhesion turnover rates (Nehru *et al.*, 2013). RhoD and Rnd1 can outcompete each other for the same binding motif in plexin A1 (Zanata *et al.*, 2002; Fansa *et al.*, 2013), a mechanism that may serve as a basis for cross-talk between the apolar and polar routes. Such cross-talk would be required in order to suppress one transition mode as the other is occurring.

Previous work suggested that there is antagonism between pro-protrusion signaling mediated by Rac1 GTPase and procontractility pathways mediated by RhoA-ROCK signaling in regulating the morphogenesis of other melanoma cell lines (Sanz-Moreno *et al.*, 2008). Our work here does not contradict this model but suggests that in WM266.4 cells the individual contributions of both RhoA and, to a lesser degree, Rac1 contribute little to cell shape in three dimensions. Instead, our results suggest a major role for RhoC, RhoB, Rac3, and other less-studied Rho GTPases, such as RhoD and RhoH, in the regulation of melanoma cell morphogenesis. RhoC is a likely upstream regulator of ROCK kinases and contractility in WM266.4 cells (Acton *et al.*, 2014; Julian and Olson, 2014), which is supported by the observation that RhoC RNAi results in large round cells that likely are poorly contractile (Figure 2), Our data suggest that Rac3 does not promote protrusions but instead promotes contractility (Hajdo-Milasinovic *et al.*, 2007, 2009). The role of other GTPases, especially those responsible for protrusion, is less clear. Whether the role of different GTPases in regulating melanoma cell shape in three dimensions is cell-line dependent and/or matrix dependent still requires investigation.

In conclusion, our work demonstrates that melanoma cells dynamically explore a more diverse shape space in 3D environments than previously believed based on qualitative studies. It remains unclear how transitions with these routes play a role in migration and ultimately metastasis of melanoma cells. In vivo the ability to use these two different routes might allow greater plasticity and ultimately increased disseminatory capability than either shape alone.

MATERIALS AND METHODS

Experimental procedures

PTEN-null WM266.4 melanoma cells from R. Marais (Paterson Institute, Manchester, United Kingdom) were maintained in DMEM plus 10% fetal bovine serum (FBS). siGENOME SMART pools (Dharmacon, Denver, CO) were used for live-cell imaging experiments. RNAi transfection was performed using RNAiMAX Lipofectamine 2000 reagent (Invitrogen, Waltham, MA) according to the manufacturer's protocol on cells cultured on plastic. Two days after transfection, cells were trypsinized and seeded on top of 50 µl of 1.7 mg/ml fibrillar bovine collagen 1 in DMEM plus 10% fetal calf serum (FCS), prepared as per manufacturer's protocol (PureCol; Advanced BioMatrix, San Diego, CA), which was aliquoted into wells of a 96-well, glass-bottomed, collagen-coated plate. Cells were allowed to adhere for 3 h, and then medium was then changed to 0% FCS. After 16 h, CellTracker orange was added as per manufacturer's protocol and cells were imaged live at 37°C at 10% CO_2 using the Opera QEHS (PerkinElmer, Waltham, MA) system, with a 20× air objective, every 5 min. Movies of up to 40 min were analyzed. At least four fields of view were captured per well, but curvature in the collagen meniscus often prevented further fields from being captured. Well repeat number also varied. The minimum repeat number was two, but often obtaining higher numbers was difficult due to the difficulty of imaging through thick collagen (Supplemental Figure S1).

During validation of phenotypes using OnTargetPlus siRNA (Dharmacon), cells were prepared as before but fixed 24 h posttransfection with 4% paraformaldehyde and stained for tubulin using anti-tubulin antibody (1:1000; A11126; Invitrogen) and nuclei using Hoescht (1:1000; H33258; Sigma-Aldrich, St. Louis, MO). Imaging was performed as described but at a single time point capturing a

30-plane *z*-stack. Maximum intensity projections were taken and used for image analysis.

Features and data preprocessing

Cells were segmented on thresholds using Acapella software (PerkinElmer). Fifteen features were recorded for each cell (Supplemental Information), many as described in Boland and Murphy (2001). Cells touching the edge were removed, and a linear classifier, manually trained, removed poorly focused/segmented cells. Tracking was performed by searching for the closest centroid in the next frame. A track would stop if a movement were greater than the cell width. Cells tracked fewer than four frames were discarded. This was carried out using in- house C++ code. In static validation, features were standardized, and cells with a feature outside five SDs were removed. All data and code are freely available at bitbucket.org/samocooper/wmpaper-data-and-code/src/d35c7dc716ba?at=master.

ACKNOWLEDGMENTS

We thank Alexis Barr, Jordan Holt, Frankie Butera, and Chris Marshall for comments on the manuscript and Robert Glen and Timothy Ebbels for comments on the data analysis. This study was supported by grants from the National Institute for Health Research Imperial Biomedical Research Centres and the STRATiGRAD graduate training program to S.C. and a Cancer Research UK Programme Foundation Award (C37275/A20146) to C.B.

REFERENCES

Acton SE, Farrugia AJ, Astarita JL, Mourao-Sa D, Jenkins RP, Nye E, Hooper S, van Blijswijk J, Rogers NC, Snelgrove KJ, *et al.* (2014). Dendritic cells control fibroblastic reticular network tension and lymph node expansion. Nature 514, 498–502.

Almendro V, Marusyk A, Polyak K (2013). Cellular heterogeneity and molecular evolution in cancer. Annu Rev Pathol 8, 277–302.

Bakal C, Aach J, Church G, Perrimon N (2007). Quantitative morphological signatures define local signaling networks regulating cell morphology. Science 316, 1753–1756.

Boland MV, Murphy RF (2001). A neural network classifier capable of recognizing the patterns of all major subcellular structures in fluorescence microscope images of HeLa cells. Bioinformatics 17, 1213–1223.

Bubeck S, Meila M, von Luxburg U (2012). How the initialization affects the stability of the k-means algorithm. ESAIM Prob Stat 16, 436–452.

Butcher DT, Alliston T, Weaver VM (2009). A tense situation: forcing tumour progression. Nat Rev Cancer 9, 108–122.

Damoulakis G, Gambardella L, Rossman KL, Lawson CD, Anderson KE, Fukui Y, Welch HC, Der CJ, Stephens LR, Hawkins PT (2014). P-Rex1 directly activates RhoG to regulate GPCR-driven Rac signalling and actin polarity in neutrophils. J Cell Sci 127, 2589–2600.

Davies DL, Bouldin DW (1979). A cluster separation measure. IEEE Trans Pattern Anal Mach Intell 2, 224–227.

Doyle AD, Wang FW, Matsumoto K, Yamada KM (2009). One-dimensional topography underlies three-dimensional fibrillar cell migration. J Cell Biol 184, 481–490.

Fansa EK, Dvorsky R, Zhang SC, Fiegen D, Ahmadian MR (2013). Interaction characteristics of Plexin-B1 with Rho family proteins. Biochem Biophys Res Commun 434, 785–790.

Friedl P, Alexander S (2011). Cancer invasion and the microenvironment: plasticity and reciprocity. Cell 147, 992–1009.

Friedl P, Wolf K (2003). Proteolytic and non-proteolytic migration of tumour cells and leucocytes. Biochem Soc Symp 277–285.

Friedl P, Wolf K (2009). Plasticity of cell migration: a multiscale tuning model. J Cell Biol 188, 11–19.

Gottesbuhren U, Garg R, Riou P, McColl B, Brayson D, Ridley AJ (2013). Rnd3 induces stress fibres in endothelial cells through RhoB. Biol Open 2, 210–216.

Gu Y, Filippi MD, Cancelas JA, Siefring JE, Williams EP, Jasti AC, Harris CE, Lee AW, Prabhakar R, Atkinson SJ, *et al.* (2003). Hematopoietic cell regulation by Rac1 and Rac2 guanosine triphosphatases. Science 302, 445–449.

Hajdo-Milasinovic A, Ellenbroek SI, van Es S, van der Vaart B, Collard JG (2007). Rac1 and Rac3 have opposing functions in cell adhesion and differentiation of neuronal cells. J Cell Sci 120, 555–566.

Hajdo-Milasinovic A, van der Kammen RA, Moneva Z, Collard JG (2009). Rac3 inhibits adhesion and differentiation of neuronal cells by modifying GIT1 downstream signaling. J Cell Sci 122, 2127–2136.

Jaffe AB, Hall A (2005). Rho GTPases: biochemistry and biology. Annu Rev Cell Dev Biol 21, 247–269.

Jones TR, Carpenter AE, Lamprecht MR, Moffat J, Silver SJ, Grenier JK, Castoreno AB, Eggert US, Root DE, Golland P, *et al.* (2009). Scoring diverse cellular morphologies in image-based screens with iterative feedback and machine learning. Proc Natl Acad Sci USA 106, 1826–1831.

Julian L, Olson MF (2014). Rho-associated coiled-coil containing kinases (ROCK): structure, regulation, and functions. Small GTPases 5, e29846.

Liu YJ, Le Berre M, Lautenschlaeger F, Maiuri P, Callan-Jones A, Heuze M, Takaki T, Voituriez R, Piel M (2015). Confinement and low adhesion induce fast amoeboid migration of slow mesenchymal cells. Cell 160, 659–672.

Nehru V, Almeida FN, Aspenstrom P (2013). Interaction of RhoD and ZIP kinase modulates actin filament assembly and focal adhesion dynamics. Biochem Biophys Res Commun 433, 163–169.

Nieto MA (2013). Epithelial plasticity: a common theme in embryonic and cancer cells. Science 342, 1234850.

Okada T, Sinha S, Esposito I, Schiavon G, Lopez-Lago MA, Su W, Pratilas CA, Abele C, Hernandez JM, Ohara M, *et al.* (2015). The Rho GTPase Rnd1 suppresses mammary tumorigenesis and EMT by restraining Ras-MAPK signalling. Nat Cell Biol 17, 81–94.

Parsons JT, Horwitz AR, Schwartz MA (2010). Cell adhesion: integrating cytoskeletal dynamics and cellular tension. Nat Rev Mol Cell Biol 11, 633–643.

Paszek MJ, Zahir N, Johnson KR, Lakins JN, Rozenberg GI, Gefen A, Reinhart-King CA, Margulies SS, Dembo M, Boettiger D, *et al.* (2005). Tensional homeostasis and the malignant phenotype. Cancer Cell 8, 241–254.

Pincus Z, Theriot JA (2007). Comparison of quantitative methods for cell-shape analysis. J Microsc 227, 140–156.

Ramo P, Sacher R, Snijder B, Begemann B, Pelkmans L (2009). CellClassifier: supervised learning of cellular phenotypes. Bioinformatics 25, 3028–3030.

Ridley AJ (2013). RhoA, RhoB and RhoC have different roles in cancer cell migration. J Microsc 251, 242–249.

Rousseeuw PJ (1987). Silhouettes: a graphical aid to the interpretation and validation of cluster analysis. J Comput Appl Math 20, 53–56.

Sahai E, Marshall CJ (2003). Differing modes of tumour cell invasion have distinct requirements for Rho/ROCK signalling and extracellular proteolysis. Nat Cell Biol 5, 711–719.

Sailem H, Bousgouni V, Cooper S, Bakal C (2014). Cross-talk between Rho and Rac GTPases drives deterministic exploration of cellular shape space and morphological heterogeneity. Open Biol 4, 130132.

Sanz-Moreno V, Gadea G, Ahn J, Paterson H, Marra P, Pinner S, Sahai E, Marshall CJ (2008). Rac activation and inactivation control plasticity of tumor cell movement. Cell 135, 510–523.

Sanz-Moreno V, Gaggioli C, Yeo M, Albrengues J, Wallberg F, Viros A, Hooper S, Mitter R, Feral CC, Cook M, *et al.* (2011). ROCK and JAK1 signaling cooperate to control actomyosin contractility in tumor cells and stroma. Cancer Cell 20, 229–245.

Shamir O, Tishby N (2008). Model selection and stability in k-means clustering. Machine Learn 80, 213–243.

Tozluoglu M, Tournier AL, Jenkins RP, Hooper S, Bates PA, Sahai E (2013). Matrix geometry determines optimal cancer cell migration strategy and modulates response to interventions. Nat Cell Biol 15, 751–762.

von Luxburg U (2010). Clustering stability: an overview. Found Trends Machine Learn 2, 235–274.

Wheeler AP, Wells CM, Smith SD, Vega FM, Henderson RB, Tybulewicz VL, Ridley AJ (2006). Rac1 and Rac2 regulate macrophage morphology but are not essential for migration. J Cell Sci 119, 2749–2757.

Yamazaki D, Kurisu S, Takenawa T (2009). Involvement of Rac and Rho signaling in cancer cell motility in 3D substrates. Oncogene 28, 1570–1583.

Yin Z, Sadok A, Sailem H, McCarthy A, Xia X, Li F, Garcia MA, Evans L, Barr AR, Perrimon N, *et al.* (2013). A screen for morphological complexity identifies regulators of switch-like transitions between discrete cell shapes. Nat Cell Biol 15, 860–871.

Zanata SM, Hovatta I, Rohm B, Puschel AW (2002). Antagonistic effects of Rnd1 and RhoD GTPases regulate receptor activity in Semaphorin 3A-induced cytoskeletal collapse. J Neurosci 22, 471–477.